DESY 08-185
SFB/CPP-08-99

DESY 08-185
SFB/CPP-08-99
December 2008

arXiv:0812.4448v1 [hep-ph] 23 Dec 2008

Determination of Strange Sea Distributions from νN Deep Inelastic Scattering

S. Alekhin[a,b,1], S. Kulagin[c,2], R. Petti[d,3]

[a]*Deutsches Elektronensynchrotron DESY*
Platanenallee 6, D–15738 Zeuthen, Germany

[b]*Institute for High Energy Physics*
142281 Protvino, Moscow region, Russia

[c]*Institute for Nuclear Research of the Academy of Sciences of Russia*
117312 Moscow, Russia

[d]*Department of Physics and Astronomy, University of South Carolina*
Columbia SC 29208, USA

Abstract

We present an analysis of the nucleon strange sea extracted from a global Parton Distribution Function fit including the neutrino and anti-neutrino dimuon data by the CCFR and NuTeV collaborations, the inclusive charged lepton-nucleon Deep Inelastic Scattering and Drell-Yan data. The (anti-)neutrino induced dimuon analysis is constrained by the semi-leptonic charmed-hadron branching ratio $B_\mu = (8.8 \pm 0.5)\%$, determined from the inclusive charmed hadron measurements performed by the FNAL-E531 and CHORUS neutrino emulsion experiments. Our analysis yields a strange sea suppression factor $\kappa(Q^2 = 20\ \mathrm{GeV}^2) = 0.62 \pm 0.04$, the most precise value available, an x-distribution of total strange sea that is slightly softer than the non-strange sea, and an asymmetry between strange and anti-strange quark distributions consistent with zero (integrated over x it is equal to 0.0013 ± 0.0009 at $Q^2 = 20\ \mathrm{GeV}^2$).

[1]**e-mail**: sergey.alekhin@ihep.ru
[2]**e-mail**: kulagin@ms2.inr.ac.ru
[3]**e-mail**: Roberto.Petti@cern.ch

1 Introduction

The strange quark (s) distribution in the nucleon is an important input for the QCD phenomenology since the contribution of the s-quarks to the hard cross sections is of the same order of magnitude as the non-strange quarks. The strange quark contribution is particularly important at small values of the parton momentum fractions x, where the quark distributions are dominated by the sea. In high-energy hadron collisions the region of $x \lesssim 0.1$ is crucial for the study of many processes and therefore an accurate determination of the strange sea is required for the interpretation of experimental data. For instance a small positive $s - \overline{s}$ asymmetry in the strange sea may help explain the anomaly in the weak mixing angle reported by the NuTeV experiment [1]. Inclusive cross sections are not very sensitive to the strange sea, since in this case the complementary contributions from strange and non-strange distributions are strongly anti-correlated. The strange sea is best constrained by the neutrino-nucleon deep-inelastic scattering (DIS) dimuon data. This process stems from the charged-current (CC) production of a charm quark, which semileptonically decays into a final state secondary muon. The charm quark production cross section involves terms proportional to both the strange and the non-strange quark distributions. However, the contributions from u- and d-quarks are suppressed by the small quark-mixing Cabibbo-Kobayashi-Maskawa (CKM) matrix elements. The most precise (anti-)neutrino dimuon data currently available are by the CCFR and NuTeV collaborations [2, 3, 4]. In this paper we describe a determination of the strange sea distributions from a global parton distribution function (PDF) fit to the hard scattering processes, such as the inclusive charged-leptons DIS and Drell-Yan data, with the inclusion of the important CCFR and NuTeV dimuon data. The analysis is performed in the next-to-next-to-leading-order (NNLO) QCD approximation for the PDF evolution and for the massless coefficient functions. The next-to-leading-order (NLO) QCD corrections to the CC heavy-quarks production cross section are taken into account. These corrections reduce theoretical uncertainties on the strange sea due to variations in the renormalization and factorization scale.

The paper is organized as follows. Section 2 presents the theoretical framework for (anti-)neutrino induced charm dimuon production. In Section 3 we discuss the result of our global fit and the dominant theoretical uncertainties in the extraction of (anti-)strange quark distributions. We also discuss the impact of the semileptonic charm quark branching ratio B_μ on the strange distributions and we present an updated value of this parameter. Comparisons of these results with the earlier determinations of the strange sea from the leading-order (LO) analysis of Ref. [3], the NLO analysis of Refs. [2, 5], and the NNLO analysis of Ref. [6] are presented. Section 4 outlines future improvements in the determination of the strange sea distributions.

2 Theoretical Framework

The differential cross section for charm quark production in CC (anti-)neutrino DIS off nucleon or nuclear target can be written as:

$$\frac{d\sigma^{(-)}_{\nu\,\mathrm{charm}}}{dxdy} = \frac{G_F^2 ME}{\pi(1+Q^2/M_W^2)^2}\left[\left(1-y-\frac{Mxy}{2E}\right)F^{(-)}_{\nu\,2,\mathrm{c}}(x,Q^2)+\right.$$
$$\left.+\frac{y^2}{2}F^{(-)}_{\nu\,\mathrm{T,c}}(x,Q^2)\pm_{(-)}y\left(1-\frac{y}{2}\right)xF^{(-)}_{\nu\,3,\mathrm{c}}(x,Q^2)\right], \quad (1)$$

where x, y, and Q^2 are common DIS variables, E is the (anti-)neutrino energy, G_F is the Fermi constant, M and M_W are the nucleon and W-boson masses, respectively, and $F_{2,T,3}$ are the corresponding structure functions (SFs). The nuclear data are usually presented in terms of an isoscalar target nucleon, which is the average over proton and neutron targets. For an isoscalar nucleon, assuming the usual isospin relations between the proton and neutron quark distributions, we have in the LO QCD approximation:

$$F^{(-)\,N}_{\nu\,2,\mathrm{c}}(x,Q^2) = 2\xi\left[|V_{cs}|^2\,\overset{(-)}{s}(\xi,\mu^2)+|V_{cd}|^2\,\frac{\overset{(-)}{u}(\xi,\mu^2)+\overset{(-)}{d}(\xi,\mu^2)}{2}\right],$$
$$F^{(-)\,N}_{\nu\,\mathrm{T,c}} = \pm_{(-)}xF^{(-)\,N}_{\nu\,3,\mathrm{c}} = \frac{x}{\xi}F^{(-)\,N}_{\nu\,2,\mathrm{c}}, \quad (2)$$

where u,d,s are the light quark distributions in the proton, $\xi = x(1+m_\mathrm{c}^2/Q^2)$ is the slow-rescaling variable appearing in the kinematics of $2\to 2$ parton scattering with one massive particle in the final state [7], and m_c is the charm quark mass. The values of the CKM matrix elements $V_{cs} = 0.97334$ and $V_{cd} = 0.2256$ [8] suggest that the strange quark contribution dominates the cross section of Eq. (1) at small x. The factorization scale μ is usually set to either Q or $\sqrt{Q^2+m_\mathrm{c}^2}$. The sensitivity to a particular choice of μ gives an idea about the impact of higher-order QCD corrections. In the NLO QCD approximation the structure functions of Eq. (2) get an additional $O(\alpha_\mathrm{s})$ contribution from the gluon-radiation and gluon-initiated processes [9]. In Fig. 1 we compare the structure functions for charm production calculated in the NLO and LO approximations. The magnitude of NLO corrections rises at small x, giving the largest effect in the case of xF_3. For realistic kinematics, the NLO corrections to Eq. (2) substantially cancel out in the difference between neutrino and anti-neutrino cross sections. In practice higher-order QCD corrections affect mainly the C-even combination $s+\bar{s}$. We calculate the QCD-evolution of PDFs in the NNLO approximation [10]. However, a fully consistent NNLO calculation of the structure functions in Eq. (1) is currently not possible, since the NNLO coefficient functions for charm quark production are not available. The contribution to NNLO corrections from the soft-gluon re-summation has been calculated in Ref. [11] and is significant only at large values of x. Therefore, we do not include these corrections in our analysis. In general, the NNLO corrections are expected to be small compared to the uncertainties of experimental data, as one can infer from the typical magnitude of NLO corrections.

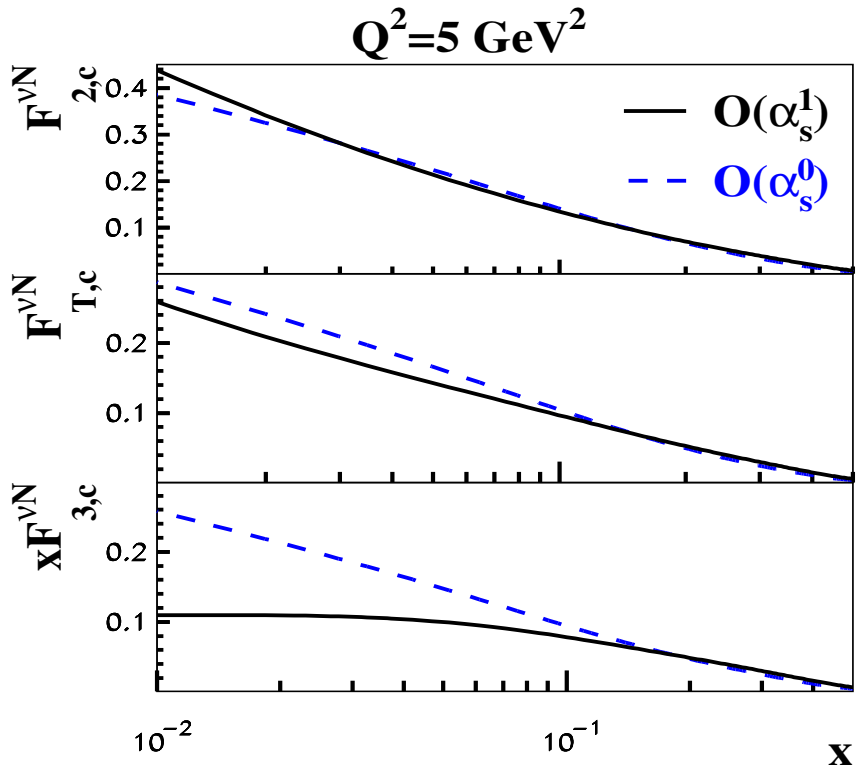

Figure 1: Comparison between LO (dashed) and NLO (solid) QCD approximations for charm quark production structure functions. The calculation is performed for neutrino interactions on isoscalar nucleons.

We do not consider power corrections to the SFs of Eq. (2). The target mass corrections of Ref. [12] are marginal in the region of $x < 0.3$ covered by the CCFR and NuTeV dimuon data. The dynamical high-twist contributions to the charm production SFs are unknown. We estimate their effect by applying a simple rescaling for the quark charge to the phenomenological twist-4 terms extracted from the inclusive νN cross-sections [13, 14]. Following this procedure we find that the impact of these corrections is negligible.

Data from the CCFR and NuTeV experiments were collected on iron target. We apply nuclear corrections to Eq. (2) using the calculation of Ref. [15, 16]. This calculation takes into account a number of different effects including the Fermi motion and binding, neutron excess, nuclear shadowing, nuclear pion excess and the off-shell correction to bound nucleon SFs. The model of Ref. [15] provides a good description of the nuclear EMC effect as measured in charged-lepton DIS over a wide range of nuclear targets, from deuterium to lead. In Ref. [16] this approach was extended to describe the (anti-)neutrino interactions with nuclei. The model predicts that nuclear corrections to the neutrino-nucleon structure functions are different from those for charged-lepton interactions. Furthermore, nuclear effects for the case of (anti-)neutrino scattering depend on the SFs type (F_2 vs. xF_3) and on the specific C-parity and isospin states. Fig. 2 shows the nuclear

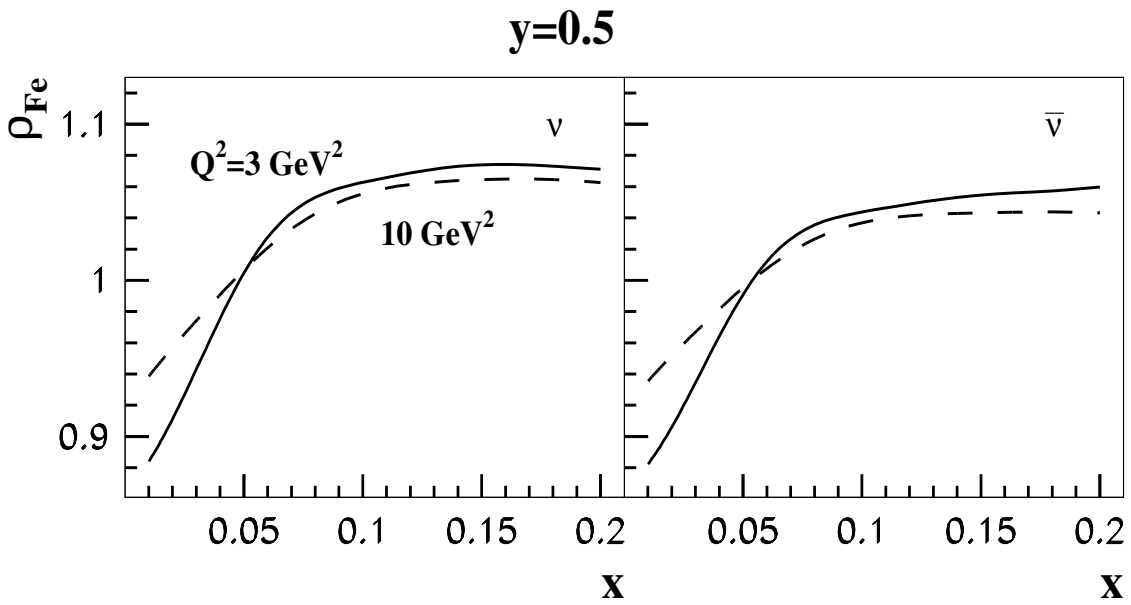

Figure 2: Ratio of differential cross sections for iron and isoscalar nucleon, $\rho_{\rm Fe}$, in neutrino (left panel) and anti-neutrino (right panel) interactions [15, 16]. The solid (dashed) curve corresponds to $Q^2 = 3\,(10)\,{\rm GeV}^2$. The inelasticity, y, is fixed at 0.5.

corrections for neutrino and anti-neutrino differential cross sections calculated for an iron target.

Electroweak corrections including the one-loop terms are calculated in Ref. [17], within the framework of the parton model, in a factorized form. In this approach the initial quark mass singularities of the QED diagrams are subtracted within the $\overline{\rm MS}$ scheme and included into the PDFs, which absorb all electroweak corrections. It is interesting to note that the electroweak and nuclear corrections are similar in magnitude in certain kinematic regions. Since the dimuon data released by the NuTeV and CCFR collaborations have already been corrected for electroweak effects according to an earlier calculation of Ref. [18], we do not apply such corrections in our fit.

In the LO the dimuon cross section is related to the corresponding cross section for charmed-quark production as:

$$\frac{d\sigma_{\mu\mu}}{dxdydz} = \frac{d\sigma_{\rm charm}}{dxdy} \sum_{\rm h} f_{\rm h} D_{\rm c}^{h}(z) Br(h \to \mu X), \tag{3}$$

where $f_{\rm h}$ is the fraction of the charmed hadron h, $D_{\rm c}^{h}(z)$ is the fragmentation function of the charm quark into a given charmed hadron $h = D^0, D^+, D_s^+, \Lambda_{\rm c}^+$ carrying a fraction z of the charm quark momentum, and $Br(h \to \mu X)$ is the corresponding inclusive branching ratio for the muon decays (note: the normalization $\sum f_{\rm h} = 1$). In the NLO the coefficient functions entering the SFs calculation depend, in general, on z as well. The charm fragmentation function $D_{\rm c}(z)$ defines the energy of the outgoing charmed hadron and, in turn, of the secondary muon produced in the semileptonic decays. Typically, a minimal energy E_μ^0 is required for the muons identified experimentally, in order to suppress the background from light-meson semileptonic decays. Assuming a universal

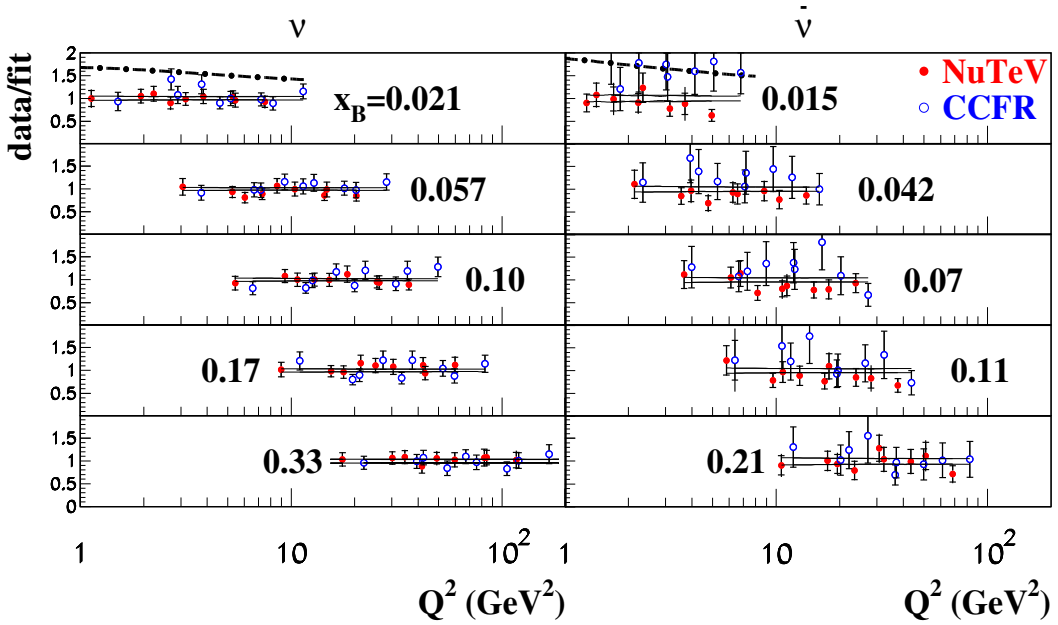

Figure 3: Pulls of CCFR and NuTeV dimuon data with respect to our fit (left panel: neutrino, right panel: anti-neutrino). The solid lines represent a $\pm 1\sigma$ band for the fitted model. The dashed dots illustrate the impact of an (anti-)strange sea enhancement on the (anti-)neutrino cross sections at small x.

$D_c(z)$ for all charmed hadrons and integrating over z, Eq. (3) reads:

$$\frac{d\sigma_{\mu\mu}(E_\mu > E_\mu^0)}{dxdy} = \eta_\mu B_\mu \frac{d\sigma_{\text{charm}}}{dxdy}, \tag{4}$$

where η_μ is the acceptance correction accounting for the cut $E_\mu > E_\mu^0$, and $B_\mu = \sum f_h Br(h \to \mu X)$ is the effective semileptonic branching ratio. We use the values of η_μ evaluated by the NuTeV and CCFR collaborations [19], which are based on the NLO calculations of Ref. [20] and on the Collins-Spiller [21] fragmentation function. The parameter ε_c, which defines the shape of $D(z)$ in the Collins-Spiller model, is fixed at 0.6. This value corresponds to the best fit value obtained in the NuTeV analysis of Ref. [19].

The charmed fractions f_h depend on the incoming neutrino energy. This fact can be explained by the contributions from quasi-elastic Λ_c and diffractive $D_s^\pm$ production. Furthermore, the values of f_h are different for neutrino and anti-neutrino beams since in the second case no quasi-elastic $\bar{\Lambda}_c$ production is present, but the relative rate of diffractive D_s production is about a factor of two larger. These two contributions are significant mainly at low energies and they would not affect the value of B_μ at $E_\nu > 40$ GeV. Measurements of f_h and B_μ in neutrino interactions were performed by the E531 [22, 23] and CHORUS [24, 25] experiments using the emulsion detection technique. A value of $B_\mu = 9.19 \pm 0.94\%$ was obtained in Ref. [23] by combining the E531 data on f_h in the energy range $E > 30$ GeV, which is relevant for the analysis of the NuTeV and CCFR dimuon data, with the charmed-hadron semileptonic branching ratios. The dominant source of uncertainty in

this determination of B_μ is related to the uncertainties on the charmed fractions $f_{\rm h}$.

A complementary determination of B_μ can be obtained from an analysis of dimuon data by performing a simultaneous fit of B_μ with other parameters [2, 3]. In such an approach the absolute value of the dimuon cross section cannot directly constrain the (anti-)strange quark sea. This contribution is rather defined by the Q^2-slope of the cross section, which is sensitive to the parton distributions through the QCD evolution equations. For anti-neutrinos the slope is driven mainly by the anti-strange sea, with a small contribution from gluons coming from the NLO corrections. In the neutrino case the non-strange quarks contribute as well. Once the (anti-)strange distributions are constrained by the Q^2-slopes, the parameter B_μ is determined by the absolute value of the dimuon (anti-)neutrino cross section. The value of B_μ obtained from this global fit can then be compared with the direct measurements from the emulsion experiments in order to check the self-consistency between the Q^2-slope and the absolute normalization of dimuon data.

3 Results

3.1 Constraints from CCFR and NuTeV Dimuon Data

We determine the strange sea distributions from a global PDF fit to the CCFR and NuTeV dimuon data of Refs. [2, 4], combined with the inclusive charged-leptons DIS and the Drell-Yan cross sections used in the earlier fit of Ref. [26]. The x-dependence of the strange and anti-strange quark distributions is parametrized independently using a model similar to that used for other PDFs:

$$x^{(-)}s\,(x,Q_0^2) = {}^{(-)}A_s\; x^{{}^{(-)}a_s}\,(1-x)^{{}^{(-)}b_s} \tag{5}$$

at the starting value of the QCD evolution $Q_0^2 = 9$ GeV^2. This functional form is flexible enough to describe the data. We do not observe any significant improvement in the quality of our fit by adding a polynomial factor to Eq. (5). The low-x exponents a_s and $\overline{a}_s$ are assumed to be the same as the one for the non-strange sea, since the existing dimuon data are not sensitive to them. The remaining parameters in Eq. (5) are extracted simultaneously with the non-strange PDF parameters, which essentially coincide with the ones obtained in Ref. [26].

Our results for the strange sea parameters are given in Table 1. The quoted uncertainties include both statistical and systematic uncertainties in the data and take into account correlations in the latter where available. We obtain values of χ^2 of 63 and 38 for the CCFR and NuTeV data sets, which both have 89 data points. It must be noted that, due to statistical correlations between data points, the effective number of degrees of freedom for the NuTeV data is about 40, which is consistent with our χ^2 value.

The ratio of CCFR and NuTeV data with respect to the fit model is given in Fig. 3. Data from both experiments are consistent and are in agreement with our fit in the whole kinematic range. Although the CCFR anti-neutrino data is higher than the model at small x, this discrepancy is within the uncertainties. The dashed curves in Fig. 3 illustrate the effect of increasing the strange

Parameter	Free B_μ	Constrained B_μ
A_s	0.086 ± 0.007	0.088 ± 0.005
a_s	-0.220 ± 0.004	-0.220 ± 0.004
b_s	7.7 ± 1.0	7.5 ± 0.5
$\overline{A}_s$	0.083 ± 0.008	0.085 ± 0.006
$\overline{a}_s$	-0.220 ± 0.004	-0.220 ± 0.004
$\overline{b}_s$	8.0 ± 0.4	7.9 ± 0.4
m_c (GeV)	1.31 ± 0.11	1.32 ± 0.11
B_μ (%)	9.1 ± 1.0	8.80 ± 0.45

Table 1: Our results for the strange sea and charm production parameters. Central column: variant of the fit in which B_μ is extracted from the CCFR and NuTeV dimuon data only; right column: variant of the fit with B_μ constrained by emulsion experiments.

sea normalization parameters A_s and $\overline{A}_s$ by 0.03 [4]. One can see that both the normalization and the Q^2-slope of the fitted model change with the strange sea normalization. If we model the energy dependence of B_μ by a linear function, the corresponding slope obtained from the fit is comparable to zero within uncertainties. We also do not observe any significant difference between the values of B_μ obtained independently from the neutrino and anti-neutrino data sets: $9.4 \pm 1.1\%$ and $8.9 \pm 2.2\%$, respectively. The neutrino-antineutrino and energy-averaged value of $B_\mu = 9.1 \pm 1.0$ % obtained in our fit is in good agreement with the results of Ref. [23]. We also extract the charm quark mass m_c from the data. We obtain a value $m_c = 1.31 \pm 0.11$ GeV, which is in agreement with the world average $\overline{MS}$ value $m_c = 1.27^{+0.07}_{-0.11}$ GeV [8].

The strange sea suppression factor

$$\kappa(Q^2) = \frac{\int_0^1 x\left[s(x,Q^2) + \overline{s}(x,Q^2)\right]dx}{\int_0^1 x\left[\overline{u}(x,Q^2) + \overline{d}(x,Q^2)\right]dx}, \tag{6}$$

calculated with the PDFs obtained from our fit is given in Fig. 4. The momenta carried by all sea quark flavors rise in the same way with Q^2, due to the QCD evolution. Therefore, the suppression factor κ also increases with Q^2. We obtain $\kappa(20\ \mathrm{GeV}^2) = 0.59 \pm 0.08$. The uncertainty in the strange sea normalization parameters is correlated with the one on B_μ. If we fix B_μ at the central value obtained in our fit, we observe a reduction by a factor of 3 in the uncertainty on κ. Our value of κ is bigger than that obtained in the NLO QCD analysis of the CCFR dimuon data [2], $\kappa(20\ \mathrm{GeV}^2) = 0.48^{+0.06}_{-0.05}$. This difference occurs since the non-strange sea quark distributions used in Ref. [2] are larger than those of both our fit and other modern sets of PDFs (Fig. 5). However, the strange sea from our fit is consistent with that of Ref. [2]. The values of κ calculated using the CTEQ6 [27] and MSTW06 [28] PDF sets agree with our determination within the uncertainties. The value of κ preferred by the combined data on the vector meson electro-production in the analysis of Ref. [29] is also consistent with our determination. The strange sea distribution obtained in our fit is

[4] We choose a shift corresponding to several standard deviations for illustration purpose.

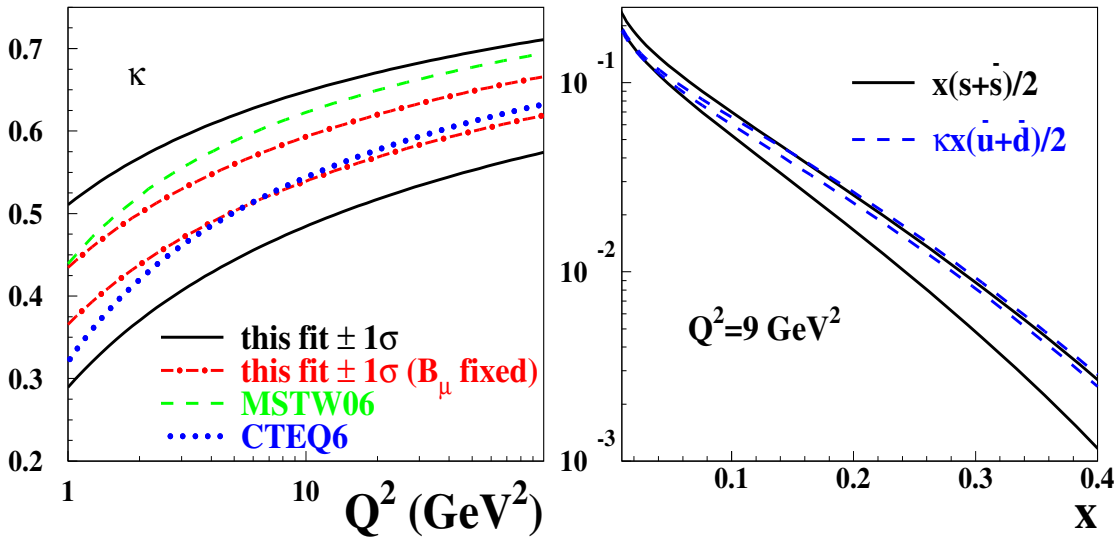

Figure 4: Left panel: The $\pm 1\sigma$ band for the strange sea suppression factor κ obtained in our fit (solid lines) compared to the determinations by the MSTW (dashes) and CTEQ (dashed dots) collaborations. The dotted lines represent the corresponding band after fixing the value of B_μ to the central value obtained in our fit, 9.1%. Right panel: The $\pm 1\sigma$ band for the C-even combination of the strange sea distributions determined in our fit (solid lines) compared to the non-strange one scaled by κ (dashes).

somewhat softer than the non-strange one (see Fig. 4). Due to the NLO corrections to the charmed-quark production coefficient functions the strange sea distributions are enhanced at small x (Fig. 6). If we do not take into account such corrections, we obtain a smaller value of $\kappa(20\ \mathrm{GeV}^2) = 0.55 \pm 0.13$. This effect is consistent with the difference between the values of κ obtained in the NLO fit of Ref. [2] and in the LO fit of Ref. [3]. The variation of the strange sea due to a change of the QCD scale μ from $\sqrt{Q^2 + m_c^2}$ to Q is smaller than the one due to the NLO correction to the charmed-quark production coefficient functions. This result indicates our fit is stable with respect to the higher-order QCD corrections.

In a variant of the fit with only the NuTeV data the strange sea is somewhat enhanced with respect to the combined CCFR and NuTeV fit (see Fig. 7). The value $B_\mu = 7.2 \pm 1.7$ % obtained in this case is correspondingly smaller than those from both the combined fit and the analysis of Ref. [23]. Although the discrepancy is at the level of 1σ, it might indicate a certain inconsistency between the Q^2-slope and the absolute normalization of the NuTeV data. In a variant of the fit with only CCFR data we get $B_\mu = 9.7 \pm 1.1$ %, which is more consistent with the results from emulsion experiments. The strange sea determined from the CCFR data is somewhat smaller than the one from the combined fit. The strange sea charge asymmetry preferred by the NuTeV data is positive at all x values and is consistent with the analysis by the NuTeV collaboration [4]. However, the CCFR data prefer negative charge asymmetry, so that the combined CCFR and NuTeV value is

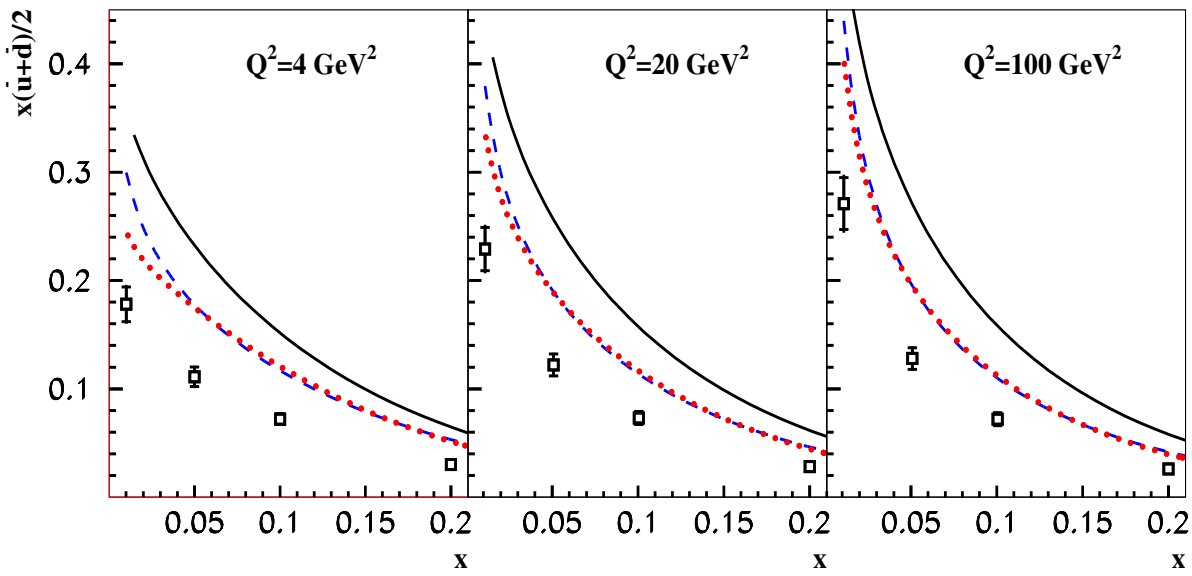

Figure 5: The non-strange sea distribution obtained in the NLO QCD fit of Ref. [2] by the CCFR collaboration (solid line) in comparison with the ones from MSTW06 (dashes) and CTEQ6 (dots) PDFs. The points give the corresponding strange-sea distribution extracted by CCFR [2].

consistent with zero at the initial scale $Q_0^2 = 9$ GeV^2 (Fig. 7). Once we impose the constraint $s(x) = \overline{s}(x)$, we observe an increase of χ^2 limited to about one unit. The variant of fit with the constraint $\int_0^1 [s(x) - \overline{s}(x)]dx = 0$ imposed also does not yield statistically significant increase in the value of χ^2.

The strange sea asymmetry rises with Q^2 [30] because of the NNLO corrections. However, even taking into account such an effect, it remains consistent with zero within uncertainties in a wide range of Q^2. In particular, at the reference scale $Q^2 = 20$ GeV^2 we obtain $S^- = \int_0^1 x[s(x) - \overline{s}(x)]dx = 0.0010(13)$. The value of S^- is sensitive to B_μ: if we fix B_μ the uncertainty on S^- is reduced by about a factor of 2. The choice of the QCD scale μ and the details of the high-order QCD corrections for the non-strange quark contributions to the charm SFs also affect S^- (Fig. 6). Changing the QCD scale μ from $\sqrt{Q^2 + m_c^2}$ to Q leads to a significant enhancement of the strange-anti-strange asymmetry at $x \sim 0.15$. The NNLO corrections to the QCD evolution and to the massless coefficient functions change the Q^2-slope of the neutrino-nucleon DIS cross section. As a result, the strange sea distributions extracted from the fit, which are sensitive to this slope, are modified and the value of the strange asymmetry decreases. The nuclear corrections, discussed in Section 2, further reduce the asymmetry at $x \sim 0.1$. Each of these factors change the value of the asymmetry within 0.5σ. A combination of the effects discussed can, in principle, explain the difference between our result and those of Refs.[5, 6], in which a positive $s - \overline{s}$ asymmetry at the level of 1-2σ was reported.

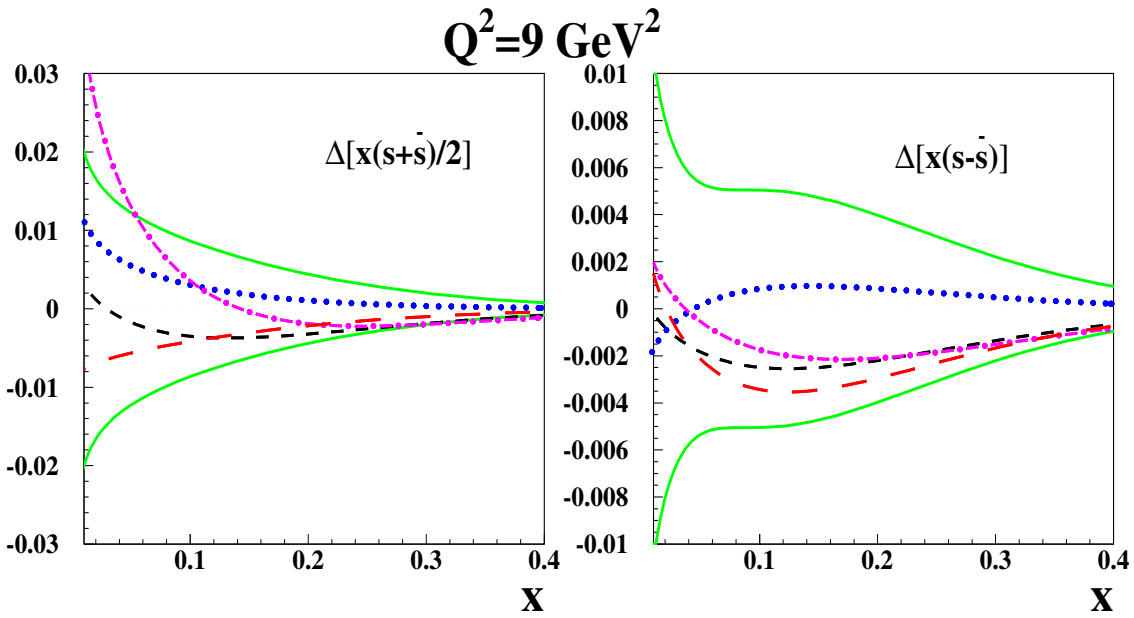

Figure 6: Sensitivity of the strange sea distribution to various corrections and settings of the fit. Left panel: The shifts in C-even $s+\overline{s}$ distribution due to the NLO QCD corrections to the charm quark production coefficient functions (dashed-dotted curve), the variation of the QCD scale μ from $\sqrt{Q^2+m_c^2}$ to Q^2 (dots), the NNLO corrections to the QCD evolution and the massless coefficient functions (long dashes), and the nuclear corrections (short dashes). The solid lines give the $\pm 1\sigma$ uncertainty band from our fit. Right panel: The same for the C-odd distribution $s-\overline{s}$.

3.2 Impact of E531 and CHORUS Emulsion Data

As explained in Section 3.1, the uncertainty on the strange sea derived from the fit can be suppressed if an additional constraint on the effective semileptonic branching ratio B_μ is imposed. Such a constrain can come from a direct detection of the charmed hadrons in the emulsion experiments. The only existing measurement of the charmed fractions f_h as a function of the neutrino energy comes from a re-analysis [23] of the data from the E531 experiment [22, 31]. Assuming μ-e universality and the recent values [8] of exclusive branching ratios for charmed hadrons we can determine B_μ at different neutrino energies. Our results for the E531 data listed in Tables 2 and 3 correspond to $B_\mu(D^0) = 6.53 \pm 0.17\%$, $B_\mu(D^+) = 16.13 \pm 0.38\%$, $B_\mu(D_s^+) = 8.06 \pm 0.76\%$ and $B_\mu(\Lambda_c^+) = 4.50 \pm 1.70\%$ [8] and take into account correlations among the measured charmed fractions [23]. Table 3 clearly shows that B_μ increases with energy, with more pronounced variations below 40 GeV. As explained in Section 2 the large contributions from quasi-elastic Λ_c and diffractive $D_s^\pm$ production at low energies explain such energy dependence. Potential differences between neutrinos and anti-neutrinos are also expected to affect mainly the region $E_\nu < 40$ GeV. This behaviour is consistent with the results of our fit to CCFR and NuTeV dimuon data described in Section 3.1.

The CHORUS experiment also measured the production rates of charmed hadrons in nuclear

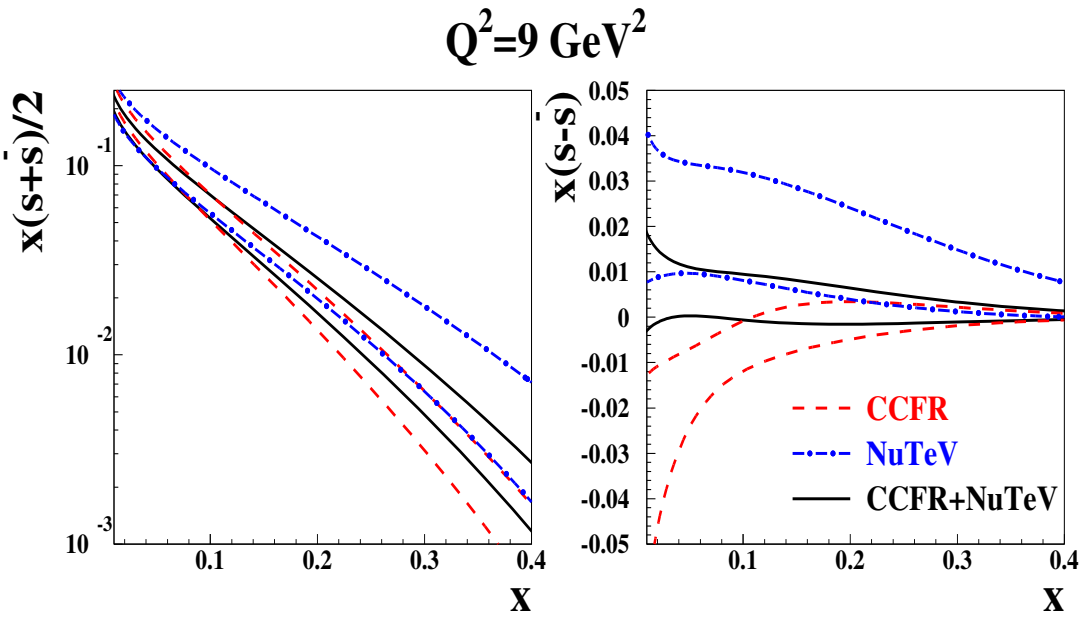

Figure 7: Left panel: $\pm 1\sigma$ bands for the C-even strange distribution $s + \bar{s}$ as obtained from the combined CCFR and NuTeV data (solid lines), from the CCFR data only (dashes), and from the NuTeV data only (dashed-dotted curves). Right panel: The same for the C-odd distribution $s - \bar{s}$.

Measurement	$E_\nu > 5$ GeV	$E_\nu > 30$ GeV
CHORUS direct [24]	7.30 ± 0.82	8.50 ± 1.08
CHORUS charmed fractions [25]	9.11 ± 0.93	
E531 charmed fractions [23]	7.86 ± 0.49	8.86 ± 0.57
Weighted average	7.94 ± 0.38	8.78 ± 0.50

Table 2: Semileptonic branching ratio B_μ(%) from direct measurements in the E531 and CHORUS emulsion experiments. The last row corresponds to our weighted average.

emulsions. Thanks to a charm statistics about 20 times higher than the one of the E531 experiment, it was possible to directly detect some of the charmed-hadrons muon decays [24]. The value of B_μ measured in Ref. [24] is given in the first line of Table 2. A second independent measurement of B_μ can be obtained by combining the inclusive charmed fractions measured in Ref. [25] with the corresponding branching ratios [8], as explained above. The result is somewhat larger than the direct measurement as can be seen from the second line of Table 2.

It is worth noting that all the determinations of B_μ from emulsion experiments are sensitive to the value of the undetectable branching ratio $D^0 \to$ all neutrals (0-prongs) [24, 32], which is decreasing the overall detection efficiency. The recent value for the fraction of 0-prong D^0 decays is $15 \pm 6\%$ [8], which is intermediate between the ones assumed by the E531 and CHORUS analyses.

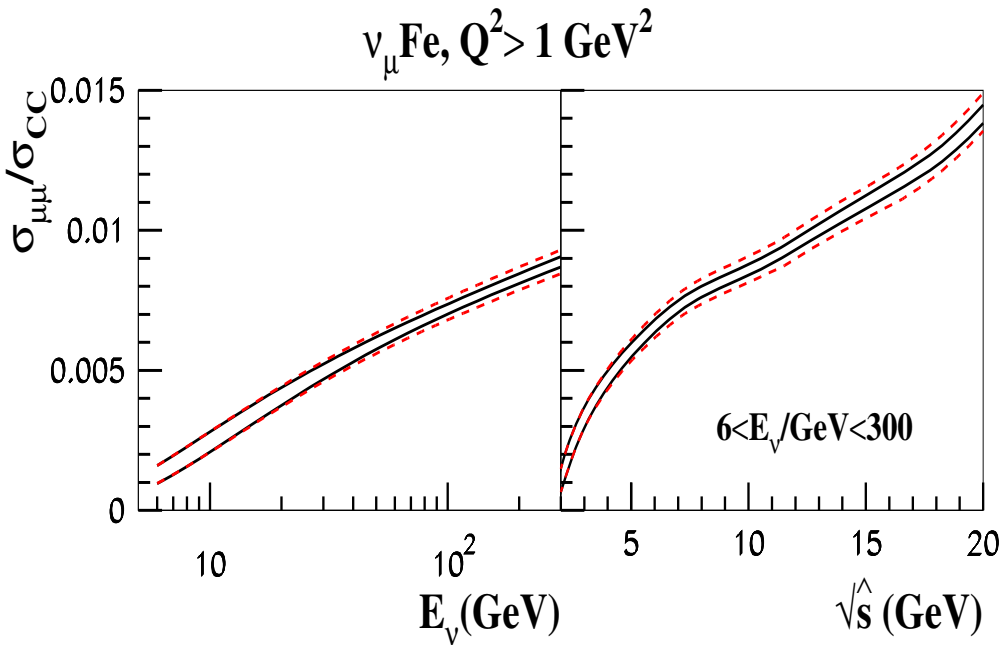

Figure 8: Left panel: The $\pm 1\sigma$ band for the ratio of the integral dimuon to the inclusive CC νFe cross sections as a function of the neutrino energy calculated using the results of our fit (solid curves). The charm production cross section ratio rescaled by the value $B_\mu = 8.8\%$ is also given for comparison (dashes). Right panel: The same for $d\sigma/d\hat{s}$, integrated over the neutrino energy spectrum of the NOMAD experiment [37] in the range of $6 \div 300$ GeV. A cut $Q^2 > 1$ GeV^2 is imposed in both cases.

Energy (GeV)	$5 < E_\nu < 20$	$20 < E_\nu < 40$	$40 < E_\nu < 80$	$E_\nu > 80$
B_μ (%)	6.33 ± 1.05	7.46 ± 0.80	8.68 ± 0.85	9.16 ± 1.33

Table 3: Semileptonic branching ratio B_μ for different neutrino energies obtained from the E531 data [23] and the recent values of inclusive leptonic branching ratios for $D^0, D^+, D_s^+, \Lambda_c^+$ [8].

We can then proceed and average all emulsion measurements (see Table 2). Uncertainties on such averaged values of B_μ are smaller than the ones obtained from our fit to the CCFR and NuTeV dimuon data. The strange sea normalization is sensitive to variations of B_μ, so that the inclusion of the emulsion data on B_μ to the fit reduces the uncertainties on the strange sea parameters. Since the energy dependence of B_μ is more pronounced at small energies we use a single constraint $B_\mu = 8.78 \pm 0.50\%$ for $E_\nu > 30$ GeV, as an additional data point in our global fit. Our independent extraction of B_μ from the CCFR and NuTeV dimuon data, $B_\mu = 9.1 \pm 1.0\%$, is consistent with such measurement. Therefore, the central value of the strange sea parameters obtained in this extended fit are comparable with those obtained if B_μ is unconstrained. However, the corresponding uncertainties are significantly reduced, as it can be seen from the second column of Table 1. The value of the strange suppression factor becomes $\kappa(20\ \text{GeV}^2) = 0.62 \pm 0.04$, with an uncertainty twice smaller as compared to the variant of the fit with B_μ unconstrained. With the constraint on B_μ we

obtain a strange sea asymmetry $S^- = 0.0013(9)$. This value is slightly larger than that obtained in the unconstrained fit, but still not significantly different from zero.

4 Summary and Outlook

In summary, we perform a global PDF fit using charged-lepton DIS data on proton and deuteron, fixed-target proton-proton and proton-deuteron Drell-Yan data, and (anti-)neutrino induced dimuon production data from CCFR and NuTeV experiments. We extract simultaneously the strange sea distributions and the effective semileptonic branching ratio B_μ for charmed hadrons. The value of B_μ obtained by our global fit is consistent with the direct measurements from the E531 and CHORUS emulsion experiments. The constraint on B_μ from emulsion data allows a reduction of the uncertainties on the strange sea parameters by about a factor of two. In particular, we obtain the absolute normalization of the strange sea with a precision of 6%, which is the most precise determination available. The x-shape of total strange sea is somewhat softer than the non-strange sea and the asymmetry between strange and anti-strange quark distributions is consistent with zero within uncertainties.

An additional constraint on the strange sea distributions can be obtained from the inclusive (anti-)neutrino CC differential cross section $d\sigma^2_{\rm CC}/dxdy$. At small values of x the scattering off strange sea quarks gives a significant contribution to the inclusive cross section. Available cross section data come from the CHORUS [33], NuTeV [34], and NOMAD [35] experiments. The impact of the inclusive νN cross sections by CHORUS on the strange sea distributions was recently studied in Ref. [36] in the context of a global PDF fit to the DIS data, resulting in a value of the asymmetry $S^- = -0.001 \pm 0.04$. The inclusive CHORUS data were also included in an extended low-Q^2 variant of our global PDF fit [13, 14].

We expect a further improvement from the forthcoming measurements of the charmed fractions and the inclusive charm production cross section by CHORUS [25]. A global analysis of existing data from E531 and CHORUS emulsion experiments will allow a determination of B_μ at a few percent level, improving the current dominant source of uncertainty on strange sea distributions.

Finally, a sample of about 15k neutrino-induced charm dimuon events is expected from the ongoing NOMAD analysis [38]. These data were collected on an iron target with an average beam energy of 24 GeV, and correspond to about three times the NuTeV dimuon statistics. Systematic uncertainties are kept well below statistical uncertainties through the measurement of the ratio of dimuon to inclusive CC cross sections, $R_{\mu\mu} = \sigma_{\mu\mu}/\sigma_{\rm CC}$, as a function of different kinematic variables. Fig. 8 shows a prediction for the NOMAD experiment based on our current results. Preliminary studies indicate that the inclusion of the NOMAD dimuon data in a global PDF fit would substantially reduce the uncertainties in the determination of the strange sea distribution. Furthermore, an accurate measurement of $R_{\mu\mu}$ as a function of the partonic center-of-mass energy squared $\hat{s} = Q^2\,(1/x - 1)$ close to the charm production threshold would allow an improved determination of the charm quark mass $m_{\rm c}$.

Acknowledgments

This work is partially supported by the RFBR grant 06-02-16659. R.P. thanks USC for supporting this research. We are grateful to D. Mason for providing the CCFR and NuTeV dimuon acceptance corrections, to A. Mitov for stimulating discussions at the early stage of this work, to F. Di Capua for discussions and clarifications about the CHORUS emulsion data, to S. Moch for the valuable comments and to S. Mishra for reading the manuscript.

References

[1] S. Davidson, S. Forte, P. Gambino, N. Rius and A. Strumia, JHEP **0202** (2002) 037 [arXiv:hep-ph/0112302].

[2] A. O. Bazarko *et al.* [CCFR Collaboration], Z. Phys. C **65** (1995) 189

[3] M. Goncharov *et al.* [NuTeV Collaboration], Phys. Rev. D **64** (2001) 112006.

[4] D. Mason *et al.*, Phys. Rev. Lett. **99** (2007) 192001.

[5] H. L. Lai, P. Nadolsky, J. Pumplin, D. Stump, W. K. Tung and C. P. Yuan, JHEP **0704**, 089 (2007)

[6] G. Watt, A. D. Martin, W. J. Stirling and R. S. Thorne, arXiv:0806.4890 [hep-ph].

[7] R. M. Barnett, Phys. Rev. Lett. **36** (1976) 1163.

[8] C. Amsler et al. [Particle Data Group], Phys. Lett. B **667** (2008) 1.

[9] T. Gottschalk, Phys. Rev. D **23** (1981) 56;
M. Gluck, S. Kretzer and E. Reya, Phys. Lett. B **380** (1996) 171 [Erratum-ibid. B **405** (1997) 391] [arXiv:hep-ph/9603304].

[10] S. Moch, J. A. M. Vermaseren and A. Vogt, Nucl. Phys. B **688** (2004) 101 [arXiv:hep-ph/0403192]; A. Vogt, S. Moch and J. A. M. Vermaseren, Nucl. Phys. B **691** (2004) 129 [arXiv:hep-ph/0404111].

[11] G. Corcella and A. D. Mitov, Nucl. Phys. B **676** (2004) 346.

[12] S. Kretzer and M. H. Reno, Phys. Rev. D **69** (2004) 034002 [arXiv:hep-ph/0307023].

[13] S. Alekhin, S. A. Kulagin and R. Petti, AIP Conf.Proc. 967 (2007) 215-224, arXiv:0710.0124 [hep-ph].

[14] S. Alekhin, S. Kulagin and R. Petti, arXiv:0810.4893 [hep-ph].

[15] S. A. Kulagin and R. Petti, Nucl. Phys. A **765**, 126 (2006) [arXiv:hep-ph/0412425].

[16] S. A. Kulagin and R. Petti, Phys. Rev. D **76**, 094023 (2007) [arXiv:hep-ph/0703033].

[17] A. B. Arbuzov, D. Y. Bardin and L. V. Kalinovskaya, JHEP **78**, 506 (2005); arXiv:hep-ph/0407203.

[18] D. Y. Bardin and V. A. Dokuchaeva, JINR-E2-86-260, Dubna, 1986.

[19] D. A. Mason, FERMILAB-THESIS-2006-01, UMI-32-11223, 2006.

[20] S. Kretzer, D. Mason and F. I. Olness, Phys. Rev. D **65**, 074010 (2002).

[21] P. D. B. Collins and T. P. Spiller, J.Phys. G 11 (1985) 1289.

[22] N. Ushida *et al.* [Fermilab E531 Collaboration], Phys. Lett. B **206** (1988) 375.

[23] T. Bolton, arXiv:hep-ex/9708014.

[24] A. Kayis-Topaksu *et al.* [CHORUS Collaboration], Phys. Lett. B **626** (2005) 24.

[25] F. Di Capua [CHORUS collaboration], Talk at Nufact08, Valencia, Spain, June 2008, http://indico.ific.uv.es/indico/conferenceOtherViews.py?view=standard&confId=71

[26] S. Alekhin, K. Melnikov and F. Petriello, Phys. Rev. D **74**, 054033 (2006).

[27] J. Pumplin, D. R. Stump, J. Huston, H. L. Lai, P. Nadolsky and W. K. Tung, JHEP **0207**, 012 (2002).

[28] A. D. Martin, W. J. Stirling, R. S. Thorne and G. Watt, Phys. Lett. B **652**, 292 (2007)

[29] S. V. Goloskokov and P. Kroll, Eur. Phys. J. C **50** (2007) 829 [arXiv:hep-ph/0611290].

[30] S. Catani, D. de Florian, G. Rodrigo and W. Vogelsang, Phys. Rev. Lett. **93** (2004) 152003 [arXiv:hep-ph/0404240].

[31] S. G. Frederiksen, PhD Thesis, FERMILAB-THESIS-1987-22.

[32] G. Onengut et al. [CHORUS collaboration], Phys. Lett. B **613** (2005) 105.

[33] G. Onengut *et al.* [CHORUS Collaboration], Phys. Lett. B **632** (2006) 65.

[34] M. Tzanov et al. [NuTeV Collaboration], Phys. Rev. D 74 (2006) 012008 [arXiv:hep-ex/0509010].

[35] R. Petti [NOMAD Collaboration], arXiv:hep-ex/0602022.

[36] J. Rojo *et al.* [NNPDF Collaboration], arXiv:0811.2288 [hep-ph].

[37] J. Altegoer et al. [NOMAD collaboration], Nucl. Instr. and Methods A 404 (1998) 96; P. Astier et al. [NOMAD collaboration], Nucl. Instr. and Methods A 515 (2003) 800.

[38] R. Petti and O. Samoylov [NOMAD collaboration], Talk at ECT workshop, Trento, Italy, October 27-30 2008, http://conferences.jlab.org/ECT08/index.html.

[39] K. P. Diener, S. Dittmaier and W. Hollik, Phys. Rev. D **69**, 073005 (2004).